A Model for Melting of an Inhomogeneous Material During Modulated Temperature Differential Scanning Calorimetry

C. V. Nikolopoulos

Department of Mathematics, Aegean University, Karlovasi, 83200, Samos, Greece

Abstract

In the present work a model considering the melting of an inhomogeneous material, such as a mixture or solution, during Modulated Temperature Differential Scanning Calorimetry (MTDSC), is derived and analysed. It is considered that during the melting of such a material a mushy region is formed and initially the behaviour of the material at the microscale is analysed. Then with the method of averaging a phase field type model is constructed for the macroscale, which consists of a system of partial differential equations and this is solved numerically. Finally the results are used to simulate the signal of MTDSC.

Key words: Modulated Temperature Differential Scanning Calorimetry (MTDSC), Heat Equation, Free boundary problems, Perturbation methods

1 Introduction

Modulated Temperature Differential Scanning Calorimetry or MTDSC is a method of measuring thermal properties of materials introduced by Reading and collaborators ([12] - [15]). In this method, conventional DSC is used with the modification that the usual programme of linear rising temperature is modulated by a periodic perturbation.

During an experiment, a sample of material under investigation is placed in one of two pans, the other of which is empty but otherwise identical, and these pans are positioned symmetrically within the calorimeter. Heat is supplied to (or removed from) the calorimeter in a controlled (and spatially) symmetric way so that the sample's temperature follows a preset programme. The temperature difference between the sample and the reference is monitored. This

gives a measure of the rate of heat intake (or output) by the sample and allows quantities such as the heat capacity to be determined. This measure of heat transfer is split into a slowly varying part, the "underlying signal", and an oscillatory part (or at least the first harmonic) the "cyclic signal". These two signals can both be used in an experiment.

In standard MTDSC, heating/cooling is done sinusoidally. Provided the amplitude is small enough, the sample also behaves linearly. This means that every quantity, $f(T_s)$ depending on temperature $T_s = bt + B\sin(\omega t)$ can be linearized and written as $f(T_s) = f(bt) + B\sin(\omega t)f'(bt)$. There will also be sinusoidal heat intake/output and all temperatures can be thought of as consisting of an underlying and a cyclic part, the latter having negligible higher harmonics.

Both the underlying and cyclic parts of the temperature are fixed by controlling heat supply. The amplitude B can be increased/reduced by varying the amplitude of the heating. There will, in general, be a phase difference between the heat supply and the temperature of the sample, and this phase will normally vary during the course of an experiment. The actual phase of the temperature is not particularly important for an analysis of the results and we shall generally take the sample temperature oscillations to be simply $B\sin(\omega t)$.

The simplest model for the calorimeter (see [8]) is given by neglecting its internal heat capacity and, without loss of generality, a pair of ordinary differential equations represents the heat flows into the pans with their associated changes of temperature:

$$\frac{dQ_s}{dt} = (C_r + C_s)\frac{dT_s}{dt} + F = K_0(T_r - T_s), \qquad \frac{dQ_r}{dt} = C_r\frac{dT_r}{dt} = K_0(T_r - T_s).$$

Here K_0 is the heat transfer coefficient between the pans and with the exterior of the calorimeter, C_r is the heat capacity of the pan, C_s is the heat capacity of the actual sample, and F is the rate of heat absorption by the sample by any chemical reaction, phase transition, etc. The temperature of the furnace T_F has been eliminated because of symmetry (see [8]).

The temperature difference of the reference and the sample, $\Delta T = (T_r - T_s)$, solves the equation

$$C_r\frac{d\Delta T}{dt} + K\Delta T = C_s\frac{dT_s}{dt} + F,$$

with $K = 2K_0$. For B small enough to allow linearization we have $\Delta T =$

$\Delta\bar{T} + \Delta\tilde{T}$ and $F = \bar{F} + \tilde{F} = \bar{F} + Re\{\hat{F}\exp i\omega t\}$ so that

$$\Delta\bar{T} = \frac{1}{K}(C_s b + \bar{F}),$$

while

$$\Delta\tilde{T} = B\omega Re\left\{\frac{C_s - i\hat{F}/B\omega}{K + i\omega C_r}e^{i\omega t}\right\}.$$

Finally the underlying and cyclic measurements of heat capacity $\bar{C}$ and $\tilde{C}$ respectively will be given by

$$\bar{C} = C_s + \bar{F}/b, \tag{1}$$
$$\tilde{C} = |C_s + \hat{F}/\omega B|, \tag{2}$$

where by, $|\cdot|$, we denote the amplitude of a quantity. To see how the melting of such an inhomogeneous material affects the output from an MTDSC run, the underlying and cyclic rate of heat absorption $\bar{F}$ and $\tilde{F}$ have to be calculated.

In reference [8] while more sophisticated models (one-dimensional, asymmetric etc.) are derived, it is shown that the basic principles of the MTDSC process are expressed fairly accurately by the simple model presented here.

In this work the focus is the behaviour of the MTDSC signal during the melting of an inhomogeneous material, such as a mixture or solution. Thus the main problem, studied here, is the modelling of the melting process inside the sample pan for such a material. In this way we can determine the heat absorption F for this specific process. Then we can use the ODE model, presented above, for the calorimeter as a whole to simulate the MTDSC signal in this case. Therefore to see how the melting of such a material affects the output from an MTDSC run, the underlying and cyclic rates of heat absorption $\bar{F}$, $\tilde{F}$ have to be determined. Knowledge of $\bar{F}$ and $\tilde{F}$ allows us to use formulas (1) and (2) and to simulate underlying and cyclic measurements.

Previous works, regarding modelling of phase transitions during MTDSC, have been done, in the case of a pure material in [8] and [11], in the case of glass transition in [5] and in the case of polymer melting in [9]. There is also interest, regarding calorimetric measurements of thermal properties of inhomogeneous materials (e.g. see [2] and the references therein). Therefore it would be useful to derive a phase field model, including microscale characteristics, in order to obtain a more accurate view of the process. In such a way we can obtain an initial idea of how the MTDSC signal is affected by the thermal properties of the material, as for example by its latent heat, during the melting process. In the present work, a simple consideration of such a phase field model, which can be solved numerically assuming spherical morphology reasonable for an

amorphous material (e.g. [2]), is derived and used for the simulation of melting during MTDSC.

More sophisticated macroscopic models for melting, derived from averaging microscopic Stefan problems, are studied in [6] and [7], where an attempt is made to indicate what sort of macroscopic models might be obtained from averaging Stefan problems, for general initial and boundary conditions. These models result in nonlinear parabolic equations for the temperature field (for the macroscale) inside the material. A more in depth application of the results in [6], and [7], in the case of melting during MTDSC, will be the subject of future work. However a simple example, of how one of these models can be adapted in the analysis for MTDSC measurements, is presented here. Note that the simulations of the MTDSC should be interpreted qualitatively.

In section 2 the melting of an inhomogeneous material, in which it is assumed that a mushy region is formed with inclusions of one phase in the other, is modelled using averaging. In this way, from solving a Stefan problem for the microstructure, we derive a phase-field type model for the macrostructure (for more about phase-field models see [3], [4]). The resulting equations form a system of partial differential equations for the underlying parts of temperature and mass fraction. Then by making the assumption of having a material of large latent heat, i.e. small Stefan number, we conclude with a simplified version of the model. This is solved numerically using a finite difference scheme in section 3.1. In section 3.2 the cyclic parts of temperature and mass fraction are obtained using numerical and asymptotic methods for large frequency and by linearizing quantities depending upon temperature. This model initially is derived by considering that the melting temperature is given by the Gibbs - Thompson condition. At a later stage the condition for the Kinetic undercooling is added in section 3.3. In section 4 we consider the case of having a material with small latent heat, i.e. Stefan number of order one, and we present the basic results of this consideration. In section 4.1 one of the models in [6] is analysed regarding an MTDSC run. Furthermore the heat flow inside the pan, for these various considerations, is calculated and is used to simulate the form of an MTDSC signal. In section 5 we conclude with a discussion about the results of this work.

2 Derivation of a Model Considering the Formation of a Mushy Region

A representation for the melting of an inhomogeneous material can be made by constructing a model which takes into account the formation of a mushy region inside the sample during the melting. The sample will be taken to be a slab (such as a thin disk) and essentially one-dimensional. The disc is symmetric

so we need to study only one half of it. The surfaces of the disk are taken to have temperature T_s controlled in the usual way, $T_s = T_o + bt + B\sin(\omega t)$ (see [8], [9], [12] - [15]). Considering now the melting process inside the sample we assume that the part of the mushy region, which is near a purely liquid zone, consists of small shrinking solid spheres imbedded in liquid and that near a purely solid zone we have small liquid spheres growing in solid. We start with the problem in the 'microscale' (this is the scale of a small sphere in the mushy region; its small size will allow us to take the temperature around it to be approximately constant). In Figure (1) we see a schematic representation of the mushy region.

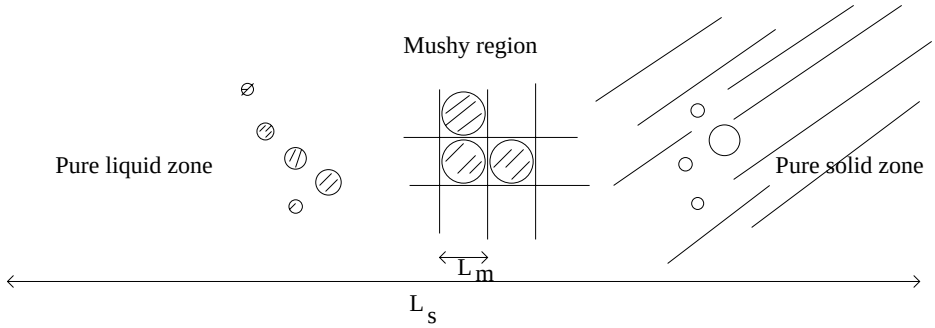

Fig. 1. Representation of a mushy region. The shaded areas are these of the solid.

The problem of the shrinking of a small solid sphere in liquid is described in more detail as follows:

In the liquid and solid parts of the mushy region the temperature T satisfies the heat equation

$$\rho c \frac{\partial T}{\partial t} = k\nabla^2 T, \tag{3}$$

where ρ is the density, c the specific heat and k the thermal conductivity. For simplicity ρ, c, k are taken to be the same for both the liquid and the solid phase. The temperature at liquid-solid interface is assumed to be given by the Gibbs-Thompson condition (see [10], [16]),

$$T_m = T_{m_o} - \sigma_S \mathcal{K}, \tag{4}$$

with σ_S being the surface tension, $\mathcal{K}$ the curvature of the interface, measured to be positive in the direction from solid to liquid, and T_{m_o} the melting temperature for a flat interface. The Stefan condition gives the motion of the boundary

$$k\left[\frac{\partial T}{\partial n}\right]_l^s = \rho \mathcal{L} V$$

where $\frac{\partial T}{\partial n}$, is the normal derivative of the temperature measured positive from the inside to the outside of the sphere, $\mathcal{L}$ the latent heat and V the speed of the boundary.

We scale time, t, temperature T, and length, x, with typical time $t_o = L_s\sqrt{\frac{\rho\mathcal{L}}{kb}}$ (L_s is the half length of the pan, i.e. we scale time with the time needed for the whole sample to melt; we need this to link this problem with the macroscopic one), $t = t_o\tau$, typical temperature $T_T = \frac{L_m^2}{L_s}\sqrt{\frac{\rho\mathcal{L}b}{k}}$, $T = T_T u$, and some intermediate length L_m (small compared with the size of the pan, i.e. $\frac{L_m}{L_s} \ll 1$), $x = L_m z$, where τ, u and z are the dimensionless time, the temperature and the space variables respectively and b is the rate of linear rise of temperature. We have scaled the variables so that we can see the effect of the latent heat, which is the dominant. Choosing this time and temperature scale we have the Stefan number, $\varepsilon^* = \frac{L_m}{L_s}\frac{cT_T}{\mathcal{L}} = \frac{L_m}{L_s}\frac{\rho c L_m^2}{t_o k} = \frac{L_m}{L_s}cL_m\sqrt{\frac{\rho b}{k\mathcal{L}}}$ which is small because of the factor $\frac{L_m}{L_s} \ll 1$, appearing in the expression for ε^*. In addition, assuming that we have a material with large latent heat, ε^* should be even smaller. In any case we take terms in ε^* negligible and this will result in having the temperature profile both in liquid and solid zones approximately harmonic. Then the temperature field both inside and outside, but near, a solid sphere is given, in spherical coordinates, by the equation

$$\frac{\partial^2 u}{\partial r^2} + \frac{2}{r}\frac{\partial u}{\partial r} = \varepsilon^*\frac{\partial u}{\partial \tau},$$

where r, is the nondimensional distance from the sphere's centre. The scaled temperature at the interface will be

$$u_m = u_0 - \frac{\sigma}{R}$$

with $\sigma = \frac{\sigma_S}{L_m T_T}$, $u_0 = \frac{T_{m_o}}{T_T}$ and R being the nondimensional radius of the solid sphere. (The dimensional radius is $R_s = L_m R$.) The Stefan condition in dimensionless form will become

$$\left[\frac{\partial u}{\partial r}\right]_l^s = \frac{\partial R}{\partial \tau}. \tag{5}$$

Assuming that the sphere's size is small compared with the scale of the spacing between the spheres in the mushy region, we can take the temperature away from a sphere, θ, as constant with respect to microscopic length scale. Therefore it depends only upon the macroscopic position and time, $\theta = \theta(y, \tau)$ for y being the scaled macroscopic position. Thus we require $u \simeq \theta(y, \tau)$ for

r large. The temperature $\theta(y,\tau)$ solves a macroscopic problem. The temperature outside and near the sphere, after solving Laplace's equation in spherical coordinates, is

$$u = \theta(y,\tau) - \frac{(\theta(y,\tau) - u_0)R + \sigma}{r}. \tag{6}$$

Note that for the temperature inside the sphere we have $\frac{\partial u}{\partial r} = 0$ because of symmetry, the fact that $\nabla^2 u = 0$, and the Gibbs-Thompson condition. This results in u being purely a function of time inside the sphere. The radius R is given by the Stefan condition, in equation (5), and by combining it with equation (6) we obtain,

$$R^2 \frac{\partial R}{\partial \tau} + (\theta(y,\tau) - u_0)R + \sigma = 0. \tag{7}$$

We now derive the macroscopic problem. We have that the temperature in the sample will satisfy the heat equation but with a heat sink due to the heat absorbed by the melting of the small solid spheres:

$$\rho c \frac{\partial T}{\partial t} = k\nabla^2 T + \rho \mathcal{L} N_s 4\pi R_s^2 \frac{\partial R_s}{\partial t}.$$

The heat sink, $\rho \mathcal{L} N_s 4\pi R_s^2 \frac{\partial R_s}{\partial t}$, is proportional to the rate of change of volume of a number N_s (measured in m^{-3}) of small solid spheres contained in a unit volume, having each one volume equals to $\frac{4\pi}{3}R_s^3$. (Volumetric heat sink= $\rho\mathcal{L}\times$rate of change of volume of a sphere$\times$number of spheres/unit volume). We now scale length with L_s, $x = L_s y$, and the rest of the variables in same way as we did for the microstructure problem and we obtain

$$\varepsilon \frac{\partial \theta}{\partial \tau} = \nabla^2 \theta + N_s 4\pi L_m^3 \left(\frac{L_s}{L_m}\right)^2 R^2 \frac{\partial R}{\partial \tau}, \tag{8}$$

where $\varepsilon = cL_s\sqrt{\frac{\rho b}{k\mathcal{L}}}$, the dimensionless Stefan number for the problem in the macroscale. It is useful for the rest of our analysis to express the radius in terms of the solid fraction. The solid fraction is related to the radius of a sphere R in the following way: $\alpha = N_s \frac{4\pi}{3} R_s^3 = N_s \frac{4\pi}{3} L_m^3 R^3$. Expressing R in terms of α we have the relations $N_s \frac{4\pi}{3} L_m^3 R^3 = \alpha$, and $N_s \frac{4\pi}{3} L_m^3 3R^2 \frac{\partial R}{\partial \tau} = \frac{\partial \alpha}{\partial \tau}$. Then the field equation takes the form

$$\varepsilon \frac{\partial \theta}{\partial \tau} = \nabla^2 \theta + \left(\frac{L_s}{L_m}\right)^2 \frac{\partial \alpha}{\partial \tau}. \tag{9}$$

Equations (9) and (7), expressing R in terms of α can be rewritten as

$$\varepsilon\frac{\partial\theta}{\partial\tau} = \nabla^2\theta(y,\tau) + C_m\frac{\partial\alpha}{\partial\tau}, \qquad \frac{\partial\alpha}{\partial\tau} + C_n(\theta(y,\tau) - u_0)\alpha^{\frac{1}{3}} + C_k = 0, \quad (10)$$

for $C_m = \left(\frac{L_s}{L_m}\right)^2$. Also $C_k = N_s 4\pi L_m^3\sigma$ and $C_n = 3^{\frac{1}{3}}\left(N_s 4\pi\right)^{\frac{2}{3}} L_m^2$.

In a similar way, near the purely solid zone we may assume that we have small liquid spheres growing in the solid. The mass of the liquid in that case is $1-\alpha$ and the corresponding equations are

$$\varepsilon\frac{\partial\theta}{\partial\tau} = \nabla^2\theta(y,\tau) + C_m\frac{\partial\alpha}{\partial\tau}, \quad \frac{\partial\alpha}{\partial\tau} + C_n(\theta(y,\tau) - u_0)(1-\alpha)^{\frac{1}{3}} - C_k = 0. \quad (11)$$

These two systems of equation express the two extreme cases of heat being absorbed in the mushy region, while in the purely liquid and purely solid zones the temperature satisfies the heat equation. From the solution of the microscopic problem near the pure liquid zone we have that the mush variation gives an effect like $\alpha^{\frac{1}{3}}$, while near the pure liquid zone it gives $(1-\alpha)^{\frac{1}{3}}$. In order to get some law for the behaviour of the mush throughout the sample we construct a function expressing the heat absorbed by the melting which near the pure liquid zone behaves like $\alpha^{\frac{1}{3}}$ and near the solid zone like $(1-\alpha)^{\frac{1}{3}}$. It should also account for the change in sign of the C_k term. A simple example of such a function f is

$$f = C_n\theta(y,\tau)\left[(1-\alpha)\alpha\right]^{\frac{1}{3}} - C_k(2\alpha - 1), \quad (12)$$

taking $u_0 = 0$, for simplicity. Indeed when α is close to zero, i.e. when we have small solid fraction, we have that $f = C_n\theta(y,\tau)\left[(1-\alpha)\alpha\right]^{\frac{1}{3}} - C_k(2\alpha - 1) \simeq C_n\theta(y,\tau)\alpha^{\frac{1}{3}} + C_k$, which is in agreement with equation (10). For α close to 1, which means that the liquid fraction is now small, we have that $f \simeq C_n\theta(y,\tau)\left(1-\alpha\right)^{\frac{1}{3}} - C_k$, which is the same as in equation (11). Therefore this function, f, has the required properties. We do this to avoid the difficulty of determining the rate law when neither solid fraction nor liquid is small (and the microscopic problem is much harder to solve).

The temperature field will be described by the system of equations

$$\varepsilon\frac{\partial\theta}{\partial\tau} = \nabla^2\theta(y,\tau) - C_m f, \quad (13)$$

$$\text{where} \qquad \frac{\partial\alpha}{\partial\tau} = -f. \quad (14)$$

The function f is defined to be:

$$f = \begin{cases} 0 & \text{in the purely liquid zone,} \\ C_n\theta(y,\tau)\left[(\alpha_c-\alpha)\alpha\right]^{\frac{1}{3}} - C_k(2\alpha-1) & \text{in the mushy region,} \\ 0 & \text{in the purely solid zone.} \end{cases} \tag{15}$$

In (15) we have accounted for no change of phase in the purely liquid ($\alpha \equiv 0$) and purely solid ($\alpha \equiv 1$) zones. We have also replaced the factor $1-\alpha$ by $\alpha_c-\alpha$, with α_c close to but greater than one to allow melting to occur (modelling nucleation); otherwise if $\alpha = 1$ initially, f as given by (12) would lead to $\alpha \equiv 1$. In the following simulation we shall take the sample to be a one-dimensional bar. At one end, $y = 0$, we take as boundary condition a linear rise of temperature, $\theta(y,\tau) = \frac{bt_o}{T_T}\tau = C_m\tau$, and we assume symmetry so that at the other end, $y = 1$, we take the temperature gradient to be zero, $\frac{\partial\theta}{\partial y} = 0$. We also take the bar to be initially solid, $\alpha(y,0) = 1$. Note that the boundary condition $\theta(y,\tau) = C_m\tau$ at $y = 0$, indicates that for the time being we drop the modulation. In the next section we will solve the problem numerically and calculate the underlying parts of temperature and solid fraction. Addition of modulation in the boundary condition and therefore the cyclic parts of temperature and solid mass fraction will be considered in section 3.2.

We may assume here that $\varepsilon \ll 1$ in the case of having large latent heat, so we may neglect terms in ε, which is a situation that we are going to consider in the next section. For example, taking some typical numbers found in [1], for a sample of amorphous silicon, and some typical parameters for MTDSC run, in [8], ($c = 1.0273 \times 10^3$ J kg^{-1o}K^{-1}, $\rho = 2.33 \times 10^3$Kg m^{-3}, $k = 0.7 \times 10^2$W m^{-1o}K^{-1}, $\mathcal{L} = 1790 \times 10^3$J kg^{-1}, $L_s = 10^{-4}$m, $b = 20$K sec^{-1}) we have $\epsilon \sim 2 \times 10^{-3} \ll 1$. We will consider the case of having $\varepsilon \sim O(1)$ in section 4. Regarding the latter we can see, by taking typical values from [2], that this can be a situation arising in solutions.

3 The case of small Stefan number ($\varepsilon \ll 1$).

Here we make the assumption that the latent heat is large so that $\varepsilon \ll 1$ and therefore we can neglect the time derivative in equation (13) which now becomes

$$\begin{aligned} & \nabla^2\theta(y,\tau) - C_m f = 0 \\ \text{or} \quad & \nabla^2\theta(y,\tau) - C_m C_n \theta(y,\tau)\left[(\alpha_c-\alpha)\alpha\right]^{\frac{1}{3}} + C_m C_k(2\alpha-1) = 0. \end{aligned} \tag{16}$$

Note that, in more detail, we could consider a perturbation expansion for θ in equation (13) , $\theta = \theta_0 + \varepsilon\theta_1 + ...$ and this gives, for $\varepsilon \ll 1$ together with the reasonable assumption that C_mC_n, C_mC_k are of order one or larger, that the resulting equation for θ_0 is equation (16). For simplicity we drop the notation of θ_0 and we write θ in the rest of this section, bearing in mind that here θ is the first order approximation of equation (13). This approximation can allow us, when $\varepsilon \ll 1$, to apply a faster in computation time numerical scheme than the one applied in section 4.

This is the most interesting case for an MTDSC run because it allows us to see the effect of temperature modulation in the MTDSC signal (we have a significant cyclic signal). As we will see in section 4, taking $\varepsilon \sim O(1)$ we have a cyclic signal which is not affected by the melting process and remains much smaller than the underlying one.

3.1 Numerical Scheme and Simulation

In order to solve the system of equations (14)-(16) we use the following procedure. Initially we have that the solid fraction is $\alpha(y, 0) = 1$ so we solve the equation (13) for $\theta(y, \tau)$ taking $\alpha = 1$. After time $\delta\tau$ the change in α will be given by the solution of equation (14), using an explicit Euler method for each space grid point: knowing θ from our previous step, say $n - 1$, we calculate α at the current, nth, time step. Then we solve (13) using a finite difference scheme for this nth time step and at the same time step we evaluate f from $\theta(y, \tau)$ and α. Then we proceed at the $(n + 1)$th time step in the same way and so on.

For the numerical solution of (13) we apply the following finite difference scheme. We divide the interval $[0, 1]$ into $S - 1$ intervals and we denote by θ_j^n and α_j^n the values of θ and α at the nth time level and at the jth space grid point. We define $f_1(\alpha_j^n) = C_n^*(\alpha_j^n(\alpha_c - \alpha_j^n))^{\frac{1}{3}}$ and $f_2(\alpha_j^n) = C_k^*(2\alpha_j^n - 1)$, where $C_n^* = C_mC_n = 3^{\frac{1}{3}}\,(N_s 4\pi)^{\frac{2}{3}}\,L_s^2$, $C_k^* = C_mC_k = N_s 4\pi L_m L_s^2 \sigma$. Also we take each space step and time step to have length δy and $\delta\tau$ respectively. With regard the boundary conditions we have that at $y = 0$ the temperature is equal to the programmed temperature at the nth time step, θ_1^n, while at $y = 1$ we have that $\frac{\partial\theta}{\partial y} = 0$. So taking an $(S + 1)$th point in the space grid we have $\theta_{S+1}^n = \theta_{S-1}^n$. Taking these relations into account at each time step we solve the system of linear equations

$$\begin{bmatrix} \delta y^2 f_1(\alpha_2^n) - 2 & 1 & & 0 \\ 1 & \delta y^2 f_1(\alpha_3^n) - 2 & \dots & 1 \\ \vdots & \vdots & \ddots & \vdots \\ 0 & \dots & 2 & \delta y^2 f_1(\alpha_{S-1}^n) - 2 \end{bmatrix} \cdot \begin{bmatrix} \theta_2 \\ \theta_3 \\ \vdots \\ \theta_{S-1} \end{bmatrix} = \begin{bmatrix} f_2(\alpha_2^n)\delta y^2 - \theta_1^n \\ f_2(\alpha_3^n)\delta y^2 \\ \vdots \\ f_2(\alpha_{S-1})^n \delta y^2 \end{bmatrix}$$

Then we obtain α_j^{n+1} using the following explicit scheme

$$\alpha_j^{n+1} = \alpha_j^n + \delta\tau \left\{ \left[-\theta_j^n C_n (\alpha_j^n (\alpha_c - \alpha_j^n))^{\frac{1}{3}} \right] + C_k (2\alpha_j^n - 1) \right\} \tag{17}$$

In the following figures, (2) and (3), the results of the simulation for an unmodulated external temperature are demonstrated. In Figure (2) we can see temperature and solid fraction against space and time. In Figure (3) in (a)

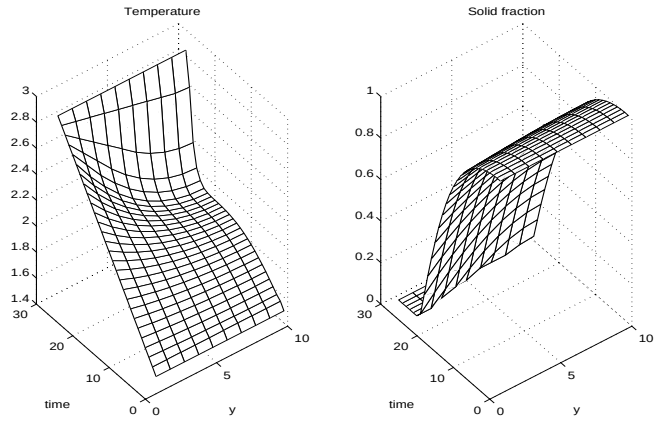

Fig. 2. Temperature and solid fraction

the solid fraction α against y, after the time that the liquid zone appears, is plotted. We see that the solid fraction decreases over time. In (b) we see the temperature profile against space for different times. It decreases with y and the stars denote the position of the free boundary at each time step. α is plotted against time for each space grid in (c). Initially α is close to one and then drops to zero starting from the point $y = 0$. Finally in (d) temperature is plotted against time for different positions. The upper line is the temperature profile at $y = 0$ and the lower one is the temperature in the middle of the pan, $y = 1$. The values taken here (and in the rest of the simulations in the following subsections) are $C_n = 1$, $C_k = 1$, $C_m = 1$ (this is rather unrealistic but we take this in order to simplify the analysis), $\alpha_c = 1.001$.

3.2 Modulation

Now we take the temperature at the left of the 'bar' with a modulated term added $\theta_S = \theta(0, \tau) = C_m \tau + lIm\{e^{i\omega_0 \tau}\}$ at $y = 0$. Note that we can linearize

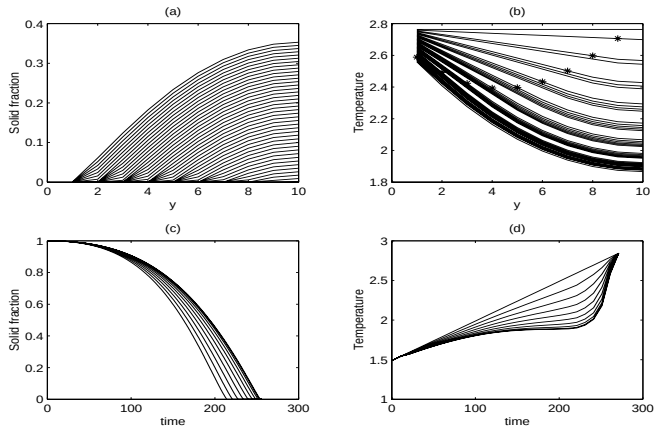

Fig. 3. Profiles of temperature and solid fraction against space and time

any quantity dependent in θ_S, for $l/C_m = B/bt_o \ll 1$ which is the case for a typical MTDSC run (see [8]).

The system of equations to be solved is again

$$\nabla^2\theta(y,\tau) + C_m\frac{\partial\alpha}{\partial\tau} = 0,$$
$$C_m\frac{\partial\alpha}{\partial\tau} = -C_n^*\theta(y,\tau)\left[(\alpha_c-\alpha)\alpha\right]^{\frac{1}{3}} + C_k^*(2\alpha-1) = -\theta(y,\tau)f_1(\alpha) + f_2(\alpha),$$

where $f_1(\alpha) = C_n^*\left[(\alpha_c-\alpha)\alpha\right]^{\frac{1}{3}}$, $f_2(\alpha) = C_k^*(2\alpha-1)$. We write the temperature θ and solid mass fraction α in the form

$$\theta = \bar{\theta}(y,\tau) + l\tilde{\theta_S} = \bar{\theta}(y,\tau) + lIm\{\hat{\theta}(y,\tau)e^{i\omega_0\tau}\}$$
$$\alpha = \bar{\alpha} + l\tilde{\alpha} = \bar{\alpha} + lIm\{\hat{\alpha}e^{i\omega_0\tau}\}$$

where $\bar{\theta}$ and $\bar{\alpha}$ denote the underlying parts, $\tilde{\theta}$ and $\tilde{\alpha}$ the cyclic, and $\hat{\theta}$ and $\hat{\alpha}$ the complex amplitudes of θ and α respectively. Substituting these expressions for θ and α into the system of equations to be solved, we obtain to the $O(1)$,

$$\frac{\partial^2\bar{\theta}(y,\tau)}{\partial y^2} + C_m\frac{\partial\bar{\alpha}}{\partial\tau} = 0, \tag{18}$$
$$C_m\frac{\partial\bar{\alpha}}{\partial\tau} = -\bar{\theta}(y,\tau)f_1(\alpha) + f_2(\alpha). \tag{19}$$

This system of equations for the underlying parts of θ and α is the same as the one solved numerically in the previous section.

The $O(l)$ terms in the system are

$$\frac{\partial^2\tilde{\theta}}{\partial y^2} + C_m\frac{\partial\tilde{\alpha}}{\partial\tau} = 0,$$
$$C_m\frac{\partial\tilde{\alpha}}{\partial\tau} = -\left[\tilde{\theta}(y,\tau)f_1(\bar{\alpha}) + \bar{\theta}(y,\tau)\tilde{\alpha}\left(\frac{df_1}{d\alpha}\right)_{\bar{\alpha}}\right] + 2C_k^*\tilde{\alpha},$$

where $\left(\frac{df_1}{d\alpha}\right)_{\bar{\alpha}} = C_n^*\left[(\alpha_c-\bar{\alpha})\bar{\alpha}\right]^{\frac{-2}{3}}(\alpha_c - 2\bar{\alpha})$. We substitute $\tilde{\theta}$ and $\tilde{\alpha}$ by $Im\{\hat{\theta}e^{i\omega_0\tau}\}$ and $Im\{\hat{\alpha}e^{i\omega\tau}\}$ respectively and we make the approximation, for large ω_0, $\frac{\partial}{\partial\tau}\left(\hat{\alpha}e^{i\omega_0\tau}\right) \simeq i\omega_0\hat{\alpha}e^{i\omega_0\tau}$. The first equation of the system becomes

$$\frac{\partial^2\hat{\theta}(y,\tau)}{\partial y^2} + iC_m\omega_0\hat{\alpha} = 0, \tag{20}$$

with $\hat{\theta} = 1$ at $y = 0$, $\frac{\partial\hat{\theta}}{\partial y} = 0$ at $y = 1$. The second equation gives for $\hat{\alpha}$,

$$\hat{\alpha}(y,\tau) = \frac{-f_1(\bar{\alpha})\hat{\theta}(y,\tau)}{\left[\left(\frac{df_1}{d\alpha}\right)_{\bar{\alpha}}\bar{\theta} + 2C_k^*\right] + iC_m\omega_0}, \tag{21}$$

and after applying the same approximation, results in a simpler algebraic equation, namely

$$\hat{\alpha}(y,\tau) = \frac{i}{C_m\omega_0}f_1(\bar{\alpha})\hat{\theta}(y,\tau). \tag{22}$$

This system of equations (20) and (22) can be solved numerically. Since $\bar{\theta}$ and $\bar{\alpha}$ are already known, we can find $\hat{\theta}$ using a finite difference scheme at each time step, and then evaluate $\hat{\alpha}$ from its algebraic relation with $\hat{\theta}$.

In Figure (4) the amplitude of temperature modulation and the amplitude of the solid fraction are plotted against space and time for $C_n^* = 1$, $C_k^* = 1$, $\alpha_c = 1.001$, $\omega_0 = 100$. We notice that $\hat{\alpha}$ is getting smaller with time, throughout the sample. Also the amplitude of the temperature, $\hat{\theta}$ initially decreases and then gradually increases till it recovers its initial value, $\hat{\alpha} = 1$, at the last time step when the melting is completed.

3.3 The Temperature at the Moving Boundary Given by the Gibbs-Thompson Condition and Kinetic Undercooling

We now take the temperature at the moving boundary to be given by the Gibbs-Thompson condition with kinetic undercooling (see [10], [16]). For small liquid spheres in solid we have that the melting temperature is

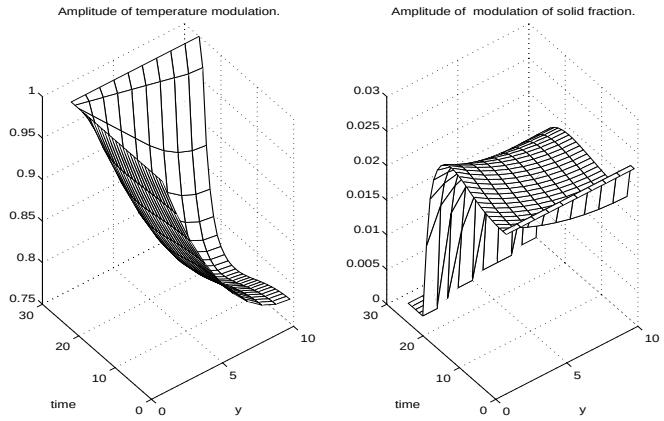

Fig. 4. Amplitudes of temperature and solid fraction

$$u_m = u_0 + \frac{\sigma}{R} + c_u \frac{\partial R}{\partial \tau}$$

for c_u a constant. The remaining equations of the small-scale problem are, again,

$$\frac{\partial^2 u}{\partial r^2} + \frac{2}{r}\frac{\partial u}{\partial r} = \varepsilon \frac{\partial u}{\partial \tau}$$
$$\text{and} \quad \left[\frac{\partial u}{\partial r}\right]_l^s = \frac{\partial R}{\partial \tau}.$$

The solution of the field equation around the sphere will be, similarly to before,

$$u = \theta(y,\tau) + \frac{\left(c_u \frac{\partial R}{\partial \tau} - (\theta(y,\tau) - u_0)\right) R + \sigma}{r}$$

and, substituting this into the Stefan condition, we have for $\frac{\partial R}{\partial \tau}$

$$\frac{\partial R}{\partial \tau}(R^2 + c_u R) = R\left(\theta(y,\tau) - u_0\right) - \sigma.$$

We express R in terms of the solid mass fraction, as previously, and we obtain the equation

$$\frac{\partial \alpha}{\partial \tau}\left(1 + C_u(1-\alpha)^{-\frac{1}{3}}\right) = -C_n(\theta(y,\tau) - u_0)(1-\alpha)^{\frac{1}{3}} + C_k,$$

with C_k and $C_u = (N_s \frac{4\pi}{3})^{-\frac{1}{3}} L_m c_u$, constants related to the surface tension and the kinetic undercooling respectively.

Finally we have

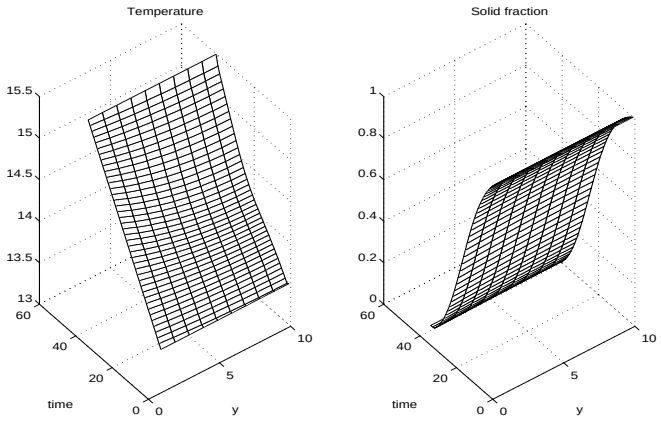

Fig. 5. Temperature and solid fraction

$$\frac{\partial \alpha}{\partial \tau} = \frac{-C_n(\theta(y,\tau) - u_0)(1-\alpha)^{\frac{1}{3}} + C_k}{\left(1 + C_u(1-\alpha)^{-\frac{1}{3}}\right)}.$$

The term $C_u(1-\alpha)^{-\frac{1}{3}}$ in the denominator is the contribution from the kinetic undercooling to the variation of α. Taking $C_u = 0$ we recover the result when the temperature at the moving boundary is given only by the Gibbs-Thompson condition.

A similar argument applies in the case of having small solid spheres in liquid and the resulting equation for α is

$$\frac{\partial \alpha}{\partial \tau} = \frac{-C_n(\theta(y,\tau) - u_0)\alpha^{\frac{1}{3}} - C_k}{\left(1 + C_u\alpha^{-\frac{1}{3}}\right)}.$$

As with the purely Gibbs-Thompson condition, to get an equation applicable everywhere, we combine the results obtained for the small liquid spheres in solid and the small solid spheres in liquid. The resulting equation is

$$\frac{\partial \alpha}{\partial \tau} = \frac{-C_n(\theta(y,\tau) - u_0)\left[\alpha(1-\alpha)\right]^{\frac{1}{3}} - C_k(1-2\alpha)}{\left(1 + C_u\left[\alpha(1-\alpha)\right]^{-\frac{1}{3}}\right)}.$$

The macroscopic problem can now be solved in exactly the same way as before. We solve the system of equations (18) and (19) but with having now the functions f_1 and f_2 being

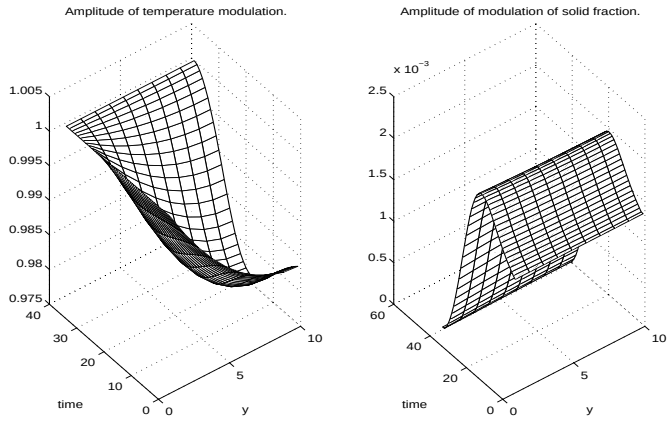

Fig. 6. Amplitudes of temperature and solid fraction

$$f_1 = \frac{C_n^*(\theta(y,\tau) - u_0)\left[\alpha(\alpha_c - \alpha)\right]^{\frac{1}{3}}}{\left(1 + C_u\left[\alpha(1-\alpha)\right]^{\frac{-1}{3}}\right)} \quad , \quad f_2 = \frac{C_k^*(1-2\alpha)}{\left(1 + C_u\left[\alpha(1-\alpha)\right]^{\frac{-1}{3}}\right)}.$$

In a similar way as before the problem is solved numerically and the results are demonstrated in the following figures, (5), (6), (7) ($C_n = C_k = C_u = 1$). We see that the results are qualitatively similar to those without kinetic undercooling. The melting process in this case is slower and this is due to the kinetic undercooling assumption.

In Figure (7) we can see a simulation of the heat flow measurement in MTDSC. The measurements for heat capacity will be given by the heat flow just inside the sample i.e. by $\frac{\partial\theta}{\partial y}(0,\tau)$. The heat absorbed by the sample will be

$$F = 2S_c k\left(\frac{\partial T}{\partial x}\right)_{x=0} = 2S_c\rho c\int_0^{L_s}\frac{\partial T}{\partial t}dx + 2S_c\mathcal{L}M\int_0^{L_s}\frac{\partial\alpha}{\partial t}dx,$$

where S_c is the cross-section area of the pan and M the mass of the sample. Therefore we have that the underlying and cyclic measurements can be obtained by formulas (1) and (2) respectively, with $\bar{F} = 2S_c k\frac{T_T}{L_s}\left(\frac{\partial\bar{\theta}}{\partial y}\right)_{y=0}$ and $\hat{F} = 2S_c k\frac{T_T}{L_s}\left(\frac{\partial\hat{\theta}}{\partial y}\right)_{y=0}$. Note that, with terms in ε neglected, the heat flows vanish unless melting is occurring. The underlying signal is always larger than the cyclic one (in the case that the melting temperature is given only by the Gibbs-Thompson condition the result is qualitatively the same). In real experiments we see this characteristic in the measurements (see [12] - [15]).

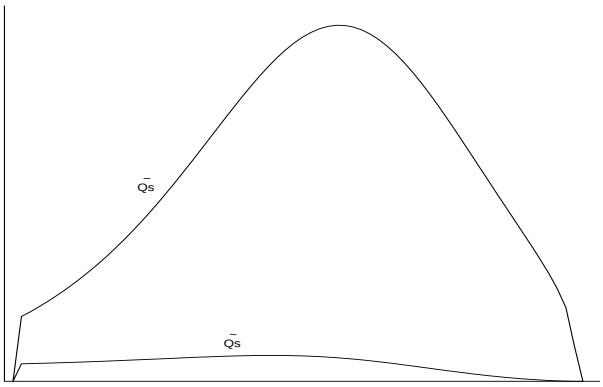

Fig. 7. Simulations of the form of heat flow measurements in the sample pan when the melting temperature is given by the Gibbs-Thompson condition with kinetic undercooling.

4 The case of having the stefan number of order one ($\varepsilon \sim \mathbf{O(1)}$).

In this case where we have a material for which $\varepsilon \sim O(1)$, the assumption of dropping the time derivative in equation (16) is no longer valid. However the model can be treated in a similar way. The equations to be solved are (13), (14) and (15). In such a case we can approximate the solution of (13) with an explicit finite difference scheme.

$$\theta_j^{n+1} = \theta_j^n + \frac{\delta\tau}{\varepsilon\delta y^2}\left(\theta_{j-1}^n - 2\theta_j^n + \theta_{j+1}^n\right) - \delta\tau\left(f_1(\alpha_j^n)\theta_j^n - f_2(\alpha_j^n)\right).$$

We pose the same boundary conditions as before, i.e. $\theta(0,\tau) = C_m\tau$ and $\frac{\partial\theta}{\partial y}(1,\tau) = 0$, and for initial condition $\theta(y,0) = \frac{\varepsilon}{2}\left((1-y)^2 - 1\right)$. The latter comes from solving the heat equation. We assume that temperature T, before melting starts, has the form $T(x,t) = \bar{T}(x) + bt + BIm\{\hat{T}(x)e^{i\omega t}\}$ for $t < 0$ (while the sample remains solid). This gives that for $t = 0$, $T(x)$ is approximately $T(x,0) \simeq -\frac{\rho cb}{2k}\left[L_s^2 - (L_s - x)^2\right]$. In this way we can obtain a numerical approximation for the underlying part of θ while at each time step α can be approximated by equation (17). The effect of keeping the time derivative in equation (13) is that the material needs more time to melt due to the heat absorption related with the heat capacity of the sample.

As regards the modulation, following the same procedure as in section 3.2 the resulting equation for the amplitude of temperature modulation is

$$\frac{\partial^2\hat{\theta}(y,\tau)}{\partial y^2} + i\omega_0\left(\frac{C_m f_1(\bar{\alpha})}{\left[\left(\frac{df1}{d\alpha}\right)_{\bar{\alpha}}\bar{\theta} - C_k^*\right] + i\omega_0} + \varepsilon\right)\hat{\theta} = 0, \tag{23}$$

with $\hat{\theta} = 0$, at $y = 0$ and $\frac{\partial \hat{\theta}}{\partial y} = 0$, at $y = 1$, while the equation for the amplitude of the solid fraction $\hat{\alpha}$ is given again by equation (21). Note that for large frequency, i.e. $\omega_0 \gg 1$ and with $\varepsilon \sim O(1)$, we have that the term multiplying $\hat{\theta}$ can be approximated by $i\omega_0\varepsilon$ so equation (23) becomes

$$\frac{\partial^2 \hat{\theta}(y,\tau)}{\partial y^2} + i\omega_0\varepsilon\hat{\theta} = 0. \tag{24}$$

This gives $\hat{\theta} = e^{-(i+1)\sqrt{\frac{\omega_0\varepsilon}{2}}}\sinh\left[(i+1)\sqrt{\frac{\omega_0\varepsilon}{2}}y\right]/\cosh\left[(i+1)\sqrt{\frac{\omega_0\varepsilon}{2}}\right] + e^{-(i+1)\sqrt{\frac{\omega_0\varepsilon}{2}}y}$. Using the numerical approximation for $\bar{\theta}$ and this expression for $\hat{\theta}$, a simulation of the MTDSC measurements is possible and this is demonstrated in Figure 8. In 8(a), the plots correspond in the case of having a Stefan number

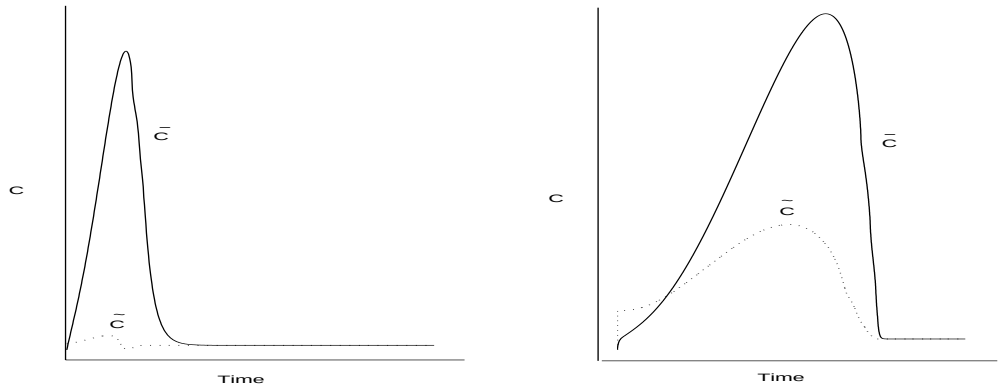

Fig. 8. Simulations of underlying (solid line) and cyclic (dotted line) forms of MTDSC measurements of heat capacity, in the case that the melting temperature is given by the Gibbs-Thompson condition.

of order one, $\varepsilon \sim 0.577$. Also $\omega_0 = 500$, $l/C_m = 0.01$, $C_n^* = 1$, $C_m^* = 1$ and $C_m = 10^3$. By increasing the frequency we would obtain a cyclic signal to be much smaller than the underlying one and being equal to the level of the heat capacity of the sample during the process. In figure 8(b), similar plots are made for ε being small ($\varepsilon = 2 \times 10^{-3}$ and the rest of the values taken are as in 8(a)) so that the approximation of neglecting the time derivative from the field equation is valid. We see that in this case (large latent heat) we have a significant cyclic signal related to the latent heat of the sample. A material with larger latent heat, and even smaller Stefan number, would affect in having even larger cyclic signal, which could possibly exceed the underlying one. Addition of the kinetic undercooling effect would have the same effects as those discussed in section 3.3.

4.1 Alternative consideration for the functional f

In order to adopt in our model more accurate forms of f we can consider the models derived in [6] and [7] which adress the full problem in the microscale in various cases. Here we present the simplest of the considerations derived in [6]. It is however more difficult to treat numerically the more advanced of the these models.

According to the simplest of these models the sample is one-dimensional medium with nucleation cites at which melting can initiate, spaced regularly, the separation of neighbouring cites being $2L_m$. The melting temperature depends only in the kinetic undercooling; $u_m = c_u V$, for c_u a constant. Following similar considerations as these presented here (for more details see [6]) the equations derived are:

$$\varepsilon \frac{\partial \theta}{\partial \tau} = \frac{\partial^2 \theta}{\partial y^2} - \frac{\partial \alpha}{\partial \tau} \tag{25}$$

$$\frac{\partial \alpha}{\partial \tau} = \begin{cases} 0, & \text{where } \theta < 0 \text{ or } \theta > 0 \text{ with } \int_{s(y)}^{\tau} \theta d\tau \geq \lambda, \\ -\frac{\theta}{\lambda}, & \text{where } \theta > 0 \text{ and } \int_{s(y)}^{\tau} \theta d\tau < \lambda, \end{cases} \tag{26}$$

with, $s(y) = \tau$, being the macroscopic free boundary separating the solid region from the mushy region (τ is the time when θ first reaches 0 at a point y), for $\lambda = C_u \frac{L_m k}{\mathcal{L} \rho L_s^2}$.

This system can be solved with a similar finite difference scheme to equations (23) and (17) but with f being $f = \frac{\theta}{\lambda}$ when melting is occurring and zero otherwise. Thus with the appropriate boundary and initial conditions we can obtain $\bar{\theta}$. With regard the amplitude of θ the usual analysis results in $\hat{\theta}$ satisfying the equation

$$\frac{\partial^2 \hat{\theta}(y,\tau)}{\partial y^2} - \left(\frac{1}{\lambda} + i\omega_0 \varepsilon \right) \hat{\theta} = 0. \tag{27}$$

Thus $\hat{\theta} = e^{-\sqrt{1/\lambda + i\omega_0}} \sinh\left[\sqrt{1/\lambda + i\omega_0} y\right] / \cosh\left[\sqrt{1/\lambda + i\omega_0}\right] - e^{-\sqrt{1/\lambda + i\omega_0} y}$. In Figure 9 the position of the macroscopic free boundaries, separating solid from mush, and mush from liquid, are plotted against time.

We can see in this simulation that there is a time period that all three phases coexist. The simulation of the MTDSC signal given by this model will give the usual bell-shape underlying measurement and a constant cyclic measurement during the melting time because $\hat{\theta}$ does not depend on the variation of $\bar{\alpha}$.

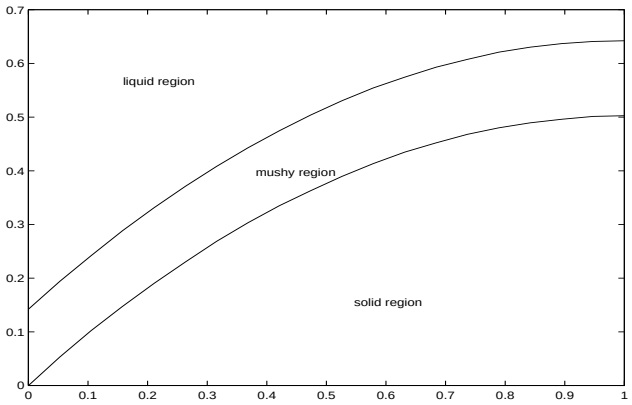

Fig. 9. Free boundaries separating the solid, mushy and liquid region during the process, for $\varepsilon = 1, \lambda = 0.1$.

5 Conclusions

A model allowing for the formation of a mushy region can be taken as a first step for the representation of the melting of a material such as a mixture, solution or an amorphous material with initially uniform solute concentration. By averaging over 'small' regions in space which contained many small spheres of one phase inside the other - with temperature given by the curvature at their interfaces - the problem can be reduced to a coupled system of differential equations for the temperature and the mass fraction of solid. These are solved numerically, initially in the case of having a small Stefan number, i.e. large latent heat, and at a later stage in the case of having a Stefan number of order one, i.e. having the effect of the latent heat comparable with that of the heat capacity of the sample. The underlying and cyclic parts of the heat flow inside the sample can then be separated, by using an asymptotic approximation for small amplitude and the underlying and cyclic measurements can be obtained. The inclusion of the kinetic undercooling in the condition for the temperature at the interface modifies slightly the model and the results are similar. It can be seen that the effect of the kinetic undercooling is to slow down the melting process, as one should expect. Also it is noted that alternative considerations, based on the same idea of averaging microscopic models, can be adopted for the analysis of the MTDSC.

The MTDSC signal is simulated and the cyclic signal appears to be smaller than the underlying one throughout the melting process. It is found that for a material with large latent heat we should expect a significant size of the cyclic signal compared to the underlying one, while in the opposite case the cyclic signal remains within the heat capacity levels of the sample.

Acknowledgment

The author wants to thank Prof. A.A. Lacey for his support and valuable advise on this work. Part of this work was completed in Heriot - Watt University under the supervision of Prof. A.A. Lacey where the author was supported by an EPSRC case award.

References

[1] J. M. Cole, P. Humphreys and L. G. Earwaker. *A Model for pulsed laser heating of Silicon.* Vacuum, **10/11**, 1984, 871-874.

[2] R. M. Devireddy, P. H. Leo, J. S. Lovengrub and J. C. Bischof. *Measurements and numerical Analysis of Freezing in solutions enclosed in a small container.* International Journal of Heat and Mass Transfer, **45**, 2002, 1915-1931.

[3] P.C. Fife, G. S. Gill *The phase phield description of mushy zones.* Physica D. **35**,1991, 267-275.

[4] P.C. Fife and O. Penrose. *Kinetics of Phase Transitions.* Lectures Notes in Physics, **84**, 210-234.

[5] K. J. Jones, I. Kinshott, M. Reading, A. A. Lacey, C. Nikolopoulos, and H. M. Pollock, *The origin and interpretation of the signals of MTDSC*, Thermochemica Acta, **304/305**, 1997, 187-199.

[6] A.A Lacey, L.A. Herraiz *Macroscopic models for melting derived from averaging microscopic Stefan problems I: Simple geometries with kinetic undercooling or surface tension* . Euro. Jnl. of Applied Mathematics, **11**, 2002 153-169.

[7] A.A Lacey, L.A. Herraiz *Macroscopic models for melting derived from averaging microscopic Stefan problems II: Effect of Varying geometry and composition.* Euro. Jnl. of Applied Mathematics, **13**, 2002, 261-282.

[8] A.A. Lacey, C. Nikolopoulos, and M. Reading. *A Mathematical Model for Modulated Differential Scanning Calorimetry.* J. Therm. Anal. **50**, 1997, 279-333.

[9] A.A. Lacey, C. Nikolopoulos. *A Model for Polymer Melting during Modulated - Temperature Differential Scanning Calorimetry.* IMA Journal of Applied Mathematics, **66**, 2001, 449-476.

[10] W. Kurtz and D.J. Fisher. *Fundamentals of Solidification.* Trans. Tech, 1986.

[11] C. Nikolopoulos. *A Model for Melting of a Pure Material During Modulated Differential Scanning Calorimetry.* SIAM J. Appl. Math. **62**, 2002, 1176-1196.

[12] M. Reading, D.Elliot and L. Hill. *Some Aspects of the Theory and Practice of Modulated Differential Scanning Calorimetry.* Proc. 21st North American Thermal Analysis Society Conference, 1992, 145-150.

[13] M. Reading. *Modulated Differential Scanning Calorimetry - A New Way Forward in Materials Characterization.* Trends in Polymer Sci., **1**, 1993, 248-253.

[14] M. Reading, A. Luget and R. Wilson. *Modulated Differential Scanning Calorimetry*, Thermochim. Acta, 1994, 238.

[15] M. Reading, R Wilson and H.M. Pollock. In Proccedings of the 23rd North American Thermal Analysis Society Conference, 1994, 2-10.

[16] D.P. Woodruff. *The Solid - Liquid Interface.* University Press Cambridge, 1973.